A travel guide to the dark matter annihilation signal

N. W. Evans
Institute of Astronomy, University of Cambridge, Madingley Road, Cambridge CB3 OHA, United Kingdom

F. Ferrer and S. Sarkar
Theoretical Physics, University of Oxford, 1 Keble Road, Oxford OX1 3NP, United Kingdom
(Received 10 September 2003; published 1 June 2004)

We provide a ''Baedecker'' or travel guide to the directions on the sky where the dark matter annihilation signal may be expected. We calculate the flux of high energy γ rays from annihilation of neutralino dark matter in the center of the Milky Way and the three nearest dwarf spheroidals (Sagittarius, Draco, and Canis Major), using realistic models of the dark matter distribution. Other investigators have used cusped dark halo profiles (such as the Navarro-Frenk-White profile) to claim a significant signal. This ignores the substantial astrophysical evidence that the Milky Way is not dark-matter dominated in the inner regions. We show that the annihilation signal from the Galactic Center falls by two orders of magnitude on substituting a cored dark matter density profile for a cusped one. The present and future generation of high energy γ-ray detectors, whether atmospheric Cherenkov telescopes or space missions such as GLAST, lack the sensitivity to detect any of the monochromatic γ-ray annihilation lines. The continuum γ-ray signal above 1 GeV and above 50 GeV may, however, be detectable either from the dwarf spheroidals or from the Milky Way itself. If the density profiles of the dwarf spheroidals are cusped, then the best prospects are for detecting Sagittarius and Canis Major. However, if the dwarf spheroidals have milder, cored profiles, then the annihilation signal is not detectable. For GLAST, an attractive strategy is to exploit the wide field of view and observe the Milky Way at medium latitudes, as suggested by Stoehr *et al.* This is reasonably robust against changes in the density profile.

DOI: 10.1103/PhysRevD.69.123501 PACS number(s): 95.35.+d

I. INTRODUCTION

The foremost candidate for the cold dark matter (CDM) composing galactic haloes is the lightest neutral supersymmetric particle, namely, the neutralino [1]. If so, then neutralino pair annihilation may lead to observable consequences, in particular the emission of high-energy γ radiation [2]. The possibility that such γ rays may be identified by forthcoming atmospheric Cerenkov telescopes (ACT) such as VERITAS [3] or by satellite-borne detectors such as GLAST [4] has excited considerable recent interest [5–8].

It is clearly of importance to identify the best places to search for such an annihilation signal. Inspired by the highly cusped models based on numerical simulations of dark halo formation [9,10], a number of investigators have suggested that the center of the Milky Way may be the optimum target. For example, Bergstrom *et al.* [2] have shown that if the dark matter density is cusped as $1/r$ at small radii, then the γ-ray flux would be detectable for typical neutralino properties in the minimal supersymmetric extension of the standard model. Inspired also by the persistence of substructure in numerical simulations, a number of authors [5,11,12] have argued that a substantial enhancement in the γ-ray signal can be expected from such ''clumps.'' In these calculations, the inner regions of the substructure are also usually assumed to be cusped. However, even within the framework of the cusped models favored by cosmological simulations, these conclusions have been contested as being overly optimistic [6].

More awkwardly, there is a substantial body of astrophysical evidence that the halo of the Milky Way is not cusped at all [13]. First, the microlensing optical depth towards the Galactic Center is very high. Particle dark matter does not cause microlensing, whereas faint stars and brown dwarfs do. The total amount of all matter within the solar circle is constrained by the rotation curve, so this tells us that lines of sight towards the Galactic Center are not dominated by particle dark matter. More specifically, haloes as strongly cusped as $1/r$, normalized to the local dark matter density as inferred from the stellar kinematics in the solar neighborhood, are ruled out by the high microlensing optical depth [14]. Second, the pattern speed of the galactic bar is known to be fast from hydrodynamical modeling of the motions of neutral and ionized gas. If dark matter dominates the central regions of the Milky Way, then dynamical friction will strongly couple the dark matter to the galactic bar and cause it to decelerate on a few bar rotation time scales [15]. It is now largely accepted by astronomers that bright galaxies such as the Milky Way do not have cusped dark haloes today, with some investigators suggesting that feedback from star formation may provide a resolution with cold dark matter theories [16].

In fact, there is *no* observational evidence whatsoever that any nearby galaxy has a cusped dark halo profile. The rotation curves of low surface brightness and dwarf spiral galaxies have been the subject of a long controversy [17,18]. The effects of beam smearing mean that the H I rotation curves of many dwarf spirals are broadly compatible with both cores and cusps. However, the H II rotation curves for at least some dwarf spirals are not compatible with cusps [19]. Most dwarf spheroidals (dSphs) do not contain gas and so the structure of the dark halos must be inferred from stellar motions. Very recently, the survival of kinematically cold sub-

TABLE I. Parameters of the dark matter halo profiles of the Draco dSph. The last three columns also give (in parentheses) the values at the location of the Sagittarius dSph. Two values are given for the tidal radius, according to whether the Milky Way halo is modeled with an isothermal power-law model or a NFW model. [Note that (1) the models sometimes require a slight velocity anisotropy in the very innermost parts to ensure everywhere physical stresses in the Jeans equation and (2) the scale radius r_s is constrained to lie below 1 kpc.]

		Cored power-law models			
α	v_a km s^{-1}	r_c kpc	r_t kpc MW-Iso	r_t kpc MW-NFW	$M(r_t) \div 10^8 M_\odot$
0.2	24.7	0.25	6.2 (2.16)	1.3 (0.5)	4.6 (2.0)
0	22.9	0.23	7.8 (2.5)	1.4 (0.51)	9.5 (3.0)
-0.2	20.9	0.21	10.1 (2.8)	1.6 (0.52)	22.43 (4.9)
		Cusped models			
0.5	2.3	0.32	6.6 (2.5)	1.5 (0.6)	5.5 (3.1)
1 (NFW)	3.3	0.62	7.0 (2.59)	1.6 (0.57)	6.6 (3.5)
1.5 (Moore)	2.9	1.0	6.5 (2.4)	1.5 (0.6)	5.5 (2.8)

structure in the Ursa Minor dSph has been used to argue against a cusped halo [20]. Hence, even at the least massive and most dark matter dominated end of the galaxy mass spectrum, the predictions of cold dark matter theories concerning halo structure seem to disagree with the observations. Nonetheless, for the three nearest dSphs—Draco, Sagittarius, and Canis Major—there is no direct evidence either for or against central cusps in their dark matter distribution.

Given this weight of evidence, it seems very prudent to use both cored and cusped halo models to estimate the range of the expected γ-ray annihilation signal. In this paper, we examine four possible locations—the Galaxy Center and the centers of the three nearest dark-matter dominated dwarf spheroidals (Draco, Sagittarius, and Canis Major). In Sec. II we use the most recent data on the velocity dispersion of the dSphs to constrain a variety of dark halo models, and in Sec. III evaluate the γ-ray flux from neutralino self-annihilations. Sections IV and V summarize the expected contribution from the background and the criterion for detection, respectively. The results for second generation ACTs and for GLAST are given in Sec. VI.

II. MODELS OF DWARF SPHEROIDALS

Dwarf spheroidals (dSphs) warrant attention because they are amongst the most extreme dark matter dominated environments. For example, the mass-to-light ratio of Draco is ~ 250 in solar units [21], while that of the Sagittarius is ~ 100 [22]. The recently discovered possible dSph in Canis Major seems similar to the Sagittarius in structural properties and dark matter content [23]. Given the seeming absence of dark matter in globular clusters, dSphs are also the smallest systems dominated by dark matter.

We develop two sets of models of dSphs. The first set is the cored spherical power-law models [24]

$$\rho_{\rm pow}(r) \equiv \frac{v_a^2 r_c^\alpha}{4\pi G} \frac{3r_c^2 + r^2(1-\alpha)}{(r_c^2 + r^2)^{2+\alpha/2}}. \tag{1}$$

Here, r_c is the core radius and v_a is a velocity scale. When $\alpha = 0$, the model has an asymptotically flat rotation curve and is the cored isothermal sphere. The rotation curves of dwarf galaxies may be gently rising or falling at large radii, so we also consider models with $\alpha = -0.2$ and 0.2, respectively.

The second set of models is the cusped haloes

$$\rho_{\rm cusp}(r) \equiv \frac{A}{r^\gamma (r + r_s)^{3-\gamma}}, \tag{2}$$

favored by numerical simulations. Here, r_s is the scale radius and A is the overall normalization. When $\gamma = 1.5$, the model is the highly cusped Moore *et al.* [9] profile, when $\gamma = 1$, the model is the Navarro-Frenk-White (NFW) profile [10]. Additionally, we study the case $\gamma = 0.5$ which represents a still milder cusped profile.

The two free parameters determining the shape of the profile are set by fitting to observational data on the Draco dSph using the Jeans equation [25]. For a spherical galaxy, the enclosed mass $M(r)$ is related to observables via

$$M(r) = -\frac{r\langle v_r \rangle^2}{G} \left(\frac{d \log \nu}{d \log r} + \frac{d \log \langle v_r^2 \rangle}{d \log r} + 2\beta \right). \tag{3}$$

Here, ν is the luminosity density, $\langle v_r^2 \rangle$ is the radial velocity dispersion of the stars and β is the anisotropy of the stellar motions. The luminosity density of Draco ν is taken as [26]

$$\nu = \frac{\nu_0 r_0^5}{(r_0^2 + r^2)^{5/2}}, \tag{4}$$

with $r_0 = 9.71' \approx 0.23$ kpc (using a heliocentric distance for Draco of 82 kpc). There are six observational points showing the line of sight velocity dispersion of Draco at different radii in Ref. [27] (using the data with no rotation subtracted). The data points are consistent with a flat profile between $2'$ and $22'$. Assuming that the anisotropy now vanishes, then the radial velocity dispersion is equal to the line-of-sight veloc-

ity dispersion. Finally, the left-hand side of Eq. (3) is fitted to the known right-hand side at the locations of the data points in Ref. [27], thus giving estimates for the two unknown parameters for each density profile as quoted in Table I.

This algorithm provides models of the Draco dSph that satisfy the available observational data. Unfortunately, the radial variation of the velocity dispersion has not been measured for the Sagittarius dSph. However, the central line-of-sight velocity dispersion of Sagittarius dSph is 11.4 km s^{-1}, very similar to that of Draco (10 km s^{-1}). Henceforth, we assume that the underlying structural parameters (v_a, r_c or A, r_s) of the Sagittarius dSph are the same as Draco. The third dSph under study—Canis Major—has only recently been claimed and the evidence for its existence is not yet clear cut. There is certainly a surprising concentration of stars in the direction of Canis Major, but this could be due to some dynamical feature such as an outer spiral arm associated with the Milky Way disk. However, for the purposes of this study, we assume the interpretation of the data in terms of a merging dSph is correct and that Canis Major dSph is similar in size and structure to Sagittarius.

To determine the extent of the dark matter halo of the dSphs, the tidal radius must be estimated. The approximate method used conventionally is derived from the Roche criterion. The tidal radius is found by requiring that the average density within the dSph is equal to the average interior density of the Milky Way halo, namely,

$$\frac{M_{\rm dSph}(r_t)}{r_t^3} = \frac{M_{\rm MW}(r_{\rm dSph} - r_t)}{(r_{\rm dSph} - r_t)^3}. \tag{5}$$

Here, $M_{\rm MW}(r)$ and $M_{\rm dSph}(r)$ are the masses enclosed within radius r of the Milky Way halo and the dwarf spheroidal, respectively, while $r_{\rm dSph}$ is the distance from the Galactic Center to the center of the dSph. We remark that this is not the same as the procedure used in a number of recent papers [8,28,29], in which the local density at the tidal radius in the dSph is set equal to the density of the background Milky Way halo at the center of the dSph.

TABLE II. The portion of the mSUGRA parameter space randomly scanned to generate the models. Here, m_0 and $m_{1/2}$ are, respectively, the common scalar and gaugino mass at the unification scale, while A_0 is the trilinear parameter and $\tan\beta$ is the ratio of the vacuum expectation values of the two Higgs fields. The μ term in the Lagrangian is allowed to have either sign.

mSUGRA parameters			
m_0 (GeV)	$m_{1/2}$ (GeV)	$\tan\beta$	$\lvert A_0\rvert$ (GeV)
10–10000	10–10000	1–60	10–10000

The results depend on the choice of profile for the Milky Way halo. For comparison purposes, we consider both a cored isothermal profile with $r_c = 10$ kpc and $v_a = 220$ km s^{-1}, and a NFW profile with concentration parameter $c = 10$. The total mass of the Milky Way halo is fixed at $M_{\rm MW} \sim 10^{12} M_\odot$, as suggested in Ref. [30]. We show in Table I the results when Eq. (5) is used to determine the tidal radius of a dSph at the locations of Draco and Sagittarius, for the two adopted models of the Milky Way halo.

III. THE γ-RAY FLUX

Let the neutralino mass be m_χ and its self-annihilation cross section be $\langle \sigma v \rangle$. Then, the γ-ray flux from neutralino annihilation is given by [2]

$$\Phi_\gamma(\psi) = \frac{N_\gamma \langle \sigma v \rangle}{4\pi m_\chi^2} \times \frac{1}{\Delta\Omega} \int_{\Delta\Omega} d\Omega \int_{\rm los} \rho^2[r(s)] ds, \tag{6}$$

TABLE III. Values of $\langle J \rangle_{\Delta\Omega}$ for the Sagittarius, Draco, and Canis Major dSphs in units of 10^{23} GeV^2 cm^{-5}. The tidal radius of the dSphs is calculated assuming an isothermal profile for the Galactic halo. Additionally, results in the direction of the Galactic Center are given for both the NFW and isothermal models of the Galactic halo.

Cored power-law models						
	Sagittarius		Draco		Canis	
α	$\Delta\Omega = 10^{-3}$ sr	$\Delta\Omega = 10^{-5}$ sr	$\Delta\Omega = 10^{-3}$ sr	$\Delta\Omega = 10^{-5}$ sr	$\Delta\Omega = 10^{-3}$ sr	$\Delta\Omega = 10^{-5}$ sr
0.2	0.6	3.4	0.07	2.2	2.4	3.4
0	0.6	3.3	0.06	2.2	2.4	3.5
−0.2	0.6	3.2	0.07	2.2	2.4	3.4
Cusped models						
	Sagittarius		Draco		Canis	
γ	$\Delta\Omega = 10^{-3}$ sr	$\Delta\Omega = 10^{-5}$ sr	$\Delta\Omega = 10^{-3}$ sr	$\Delta\Omega = 10^{-5}$ sr	$\Delta\Omega = 10^{-3}$ sr	$\Delta\Omega = 10^{-5}$ sr
0.5	1.1	17.8	0.1	5.7	6.2	32.3
1 (NFW)	1.3	36.9	0.1	7.2	8.3	139.9
1.5 (Moore)	7.3	615.1	0.6	55.4	49.1	5469
Galactic center						
Profile	$\Delta\Omega = 10^{-3}$ sr	$\Delta\Omega = 10^{-5}$ sr				
NFW, $\gamma = 1$	26	280				
Cored, $\alpha = 0$	0.3	0.3				

where ρ is the density of the dSph as a function of distance from its center r, which, of course, depends on the heliocentric distance s. The integration is performed along the line of sight to the target and averaged over the solid angle $\Delta\Omega$ of the detector. In particular, $N_\gamma=2$ for the annihilation of two nonrelativistic neutralinos into two photons ($\chi\bar{\chi}\to\gamma\gamma$) and $N_\gamma=1$ for the annihilation into a photon and a Z boson ($\chi\bar{\chi}\to Z\gamma$). The first part of the integrand (6) depends on the particular particle physics model for neutralino annihilations. The second part is a line-of-sight integration through the dark matter density distribution. We discuss each in detail in the next two subsections.

A. Particle physics model

To compute $N_\gamma\langle\sigma v\rangle/(4\pi m_\chi^2)$, we have to select a supersymmetric model. We focus on minimal supergravity (mSUGRA) models with universal gaugino and scalar masses and trilinear terms at the unification scale [31]. We use the computer program SOFTSUSY [32] to scan the supersymmetric parameter space (see Table II) and generate 10^5 models which have consistent electroweak symmetry breaking and grand unification. The output at the electroweak scale is fed into the program DARKSUSY [33] which computes the relic density and products of the neutralino annihilations. It also checks that a given model is not ruled out by present accelerator experiments.

A feasible model is one which is permitted by accelerator limits and which predicts a relic density in the range $0.005<\Omega_{\rm CDM}h^2<0.2$. This is somewhat broader than the range $0.09<\Omega_{\rm CDM}h^2<0.13$ determined by fitting the standard ΛCDM model to the WMAP data [34]. This is done so as to incorporate the higher values for $\Omega_{\rm CDM}h^2$ found for consistent alternative CDM models [35]. The lower limit is set by requiring the relic particle to provide most of the dark matter in galaxies (taking a typical mass-to-light ratio for galaxies of ~ 10, cf. the critical mass to light ratio of ~ 2000 in solar units). The range of the supersymmetric parameters scanned are given in Table II. For each feasible model, we record the quantities $N_\gamma\langle\sigma v\rangle$ for the discrete lines $\chi\chi\to\gamma\gamma$ and $\chi\chi\to Z\gamma$, as well as the continuous γ-ray spectrum above 1 and 50 GeV. Note that in the previous study [2], the relic density was much less constrained and models with arbitrary low values were permitted.

B. Line-of-sight integration of dark matter density

The line-of-sight integration can be manipulated thus:

$$\langle J\rangle_{\Delta\Omega}\doteq\frac{1}{\Delta\Omega}\int_{\Delta\Omega}J(\psi)\,{\rm d}\Omega$$

$$=\frac{2\pi}{\Delta\Omega}\int_0^{\theta_{\rm max}}{\rm d}\theta\sin\theta\int_{s_{\rm min}}^{s_{\rm max}}{\rm d}s\rho^2(\sqrt{s^2+s_0^2-2ss_0\cos\theta}), \tag{7}$$

where

$$J(\psi)=\int_{\rm los}ds\rho^2(r). \tag{8}$$

In these formulas, angled brackets denote the averaging over the solid angle $\Delta\Omega$, while $s_{\rm min}$ and $s_{\rm max}$ are the lower and upper limits of the line-of-sight integration, given by $s_0\cos\theta\pm\sqrt{r_t^2-s_0^2\sin^2\theta}$. Here, s_0 is the heliocentric distance of the dSph and r_t is the tidal radius of the dSph. Finally, $\theta_{\rm max}$ is the angle over which we average around the center of the dSph. It generally is, at least, equal to the experimental resolution and can be fixed using

$$\Delta\Omega=2\pi\int_0^{\theta_{\rm max}}d\theta\sin\theta=2\pi[1-\cos(\theta_{\rm max})].$$

The quoted point spread function widths for the various experiments are 0.4° (EGRET), 0.1° (GLAST, HESS and VERITAS), 0.15°−0.04° (CANGAROO-III). EGRET and GLAST are satellite detectors with low energy thresholds ($\approx$100 MeV), high-energy resolution ($\approx$15%) but only moderate angular precision. The others are ACTs with higher thresholds ($\approx$100 GeV) but better angular resolution. Typical reference sizes for the solid angle are $\Delta\Omega=10^{-5}$ sr for ACTs and GLAST and $\Delta\Omega=10^{-3}$ sr for EGRET.

Table III lists values of $\langle J\rangle_{\Delta\Omega}$ for the dSph profiles introduced in Sec. II. The heliocentric distances to the Draco, Sagittarius, and Canis Major dSphs are $\sim$80, 24, and 8 kpc, respectively, and this largely controls the relative values of $\langle J\rangle_{\Delta\Omega}$ for the three dSphs. Clearly, the comparative closeness of the Canis Major dSph works to its advantage as a possible target. An increase in angular sensitivity enhances the signal for all three dSphs. We remark that, in the literature, there is a considerable spread in the values obtained for $\langle J\rangle_{\Delta\Omega}$ for different sources. In Ref. [7], a one-component King profile was used to model the dSph density distribution. These authors only give explicit estimates of the entire line-of-sight integral. However, the values are of the order of 10^{21} GeV^2 cm^{-5}, lower than those implied by Table III. In Ref. [8], no angular average is taken, but instead the approximation

$$J\approx\frac{\int_{\rm los}\rho^2(l)dl}{4\pi d^2}, \tag{9}$$

is used, together with an singular isothermal profile for Draco. Taking the value given for $m_\chi=100$ GeV implies 3.7×10^{20} GeV^2 cm^{-5} for the line-of-sight integral. It is surprisingly low and yet the plots manage to exclude as large a region in parameter space as in Ref. [2]. As we discuss in Sec. V, the reason for this is the criterion used in Ref. [8] to identify a detectable signal.

As seen in the bottom panel of Table III, the γ-ray emission towards the Galactic Center falls by at least two orders of magnitude on moving from a cusped NFW halo to a cored isothermal model. The point that the signal from the Galactic

TABLE IV. This gives flux values in physical units of photons $\mathrm{cm}^{-2}\ \mathrm{s}^{-1}$ for the Galactic Center and the three dSphs, assuming a field of view of 3°. These numbers are computed from the values of $\langle J\rangle$ given in Table III under further assumptions of characteristic values for the neutralino mass and cross section (viz., $m_\chi = 100$ GeV and $N_\gamma\langle\sigma v\rangle = 10^{-25}\ \mathrm{cm}^3\ \mathrm{s}^{-1}$). In each case, results for a cusped NFW ($\gamma=1$) and a cored power-law ($\alpha=0$) model are given.

	Flux values (in photons cm^{-2})			
Model	Galactic Center	Sagittarius dSph	Draco dSph	Canis Major dSph
NFW	3.2×10^{-9}	1.1×10^{-10}	9.9×10^{-12}	7.8×10^{-10}
Power law	6.0×10^{-11}	5.3×10^{-11}	5.1×10^{-12}	2.9×10^{-10}

Center depends sensitively on the assumed halo profile, and so may have been overestimated, has also been made recently by Stoehr *et al.* [6]. For example, an optimistic result for the γ-ray flux towards the Galactic Center was obtained in Ref. [2] by using a cusped NFW model normalized to satisfy two constraints on the halo mass M and circular speed v_h, namely,

$$M(r<100\ \ \mathrm{kpc}) = (6.3\pm2.5)\times10^{11} M_\odot,$$

$$v_h(R_0) \approx 128-207\ \ \mathrm{km\ s}^{-1}. \tag{10}$$

If the normalization is set to obtain the maximum flux (as is done, for example, in Fig. 9 of Ref. [2]), then the models possess a local dark matter density substantially in excess of the usual value of $\sim 0.3\ \mathrm{GeV\ cm}^{-3}$. Anyhow, even accepting the debatable proposition that the Galaxy did once have a pristine dark halo of the NFW form, the formation of the Galactic disk, bulge and bar will have substantially reprocessed the dark matter distribution. Certainly, the evidence from the microlensing optical depth towards the Galactic Center and the pattern speed of the galactic bar are inconsistent with models dominated by dark matter in the central regions [13].

Finally, let us illustrate how to convert the numbers in Table III into photon fluxes. This requires adopting characteristic values for the particle physics parameters; here, we take $m_\chi = 100$ GeV and $N_\gamma\langle\sigma v\rangle = 10^{-25}\ \mathrm{cm}^3\ \mathrm{s}^{-1}$ for energies in excess of 1 GeV. Assuming the field of view is fixed at 3° (in other words, the semiangle of the cone whose axis points towards the center of the objects is 1.5°), the implied photon fluxes from the Sagittarius, Draco, and Canis Major dSphs are as given in Table IV.

IV. COMPUTATION OF THE BACKGROUND

There are three sources of background for the signal under consideration: hadronic, cosmic-ray electrons, and diffuse γ rays from astrophysical processes. The last is negligible for ACTs, but is the only one present for satellite experiments such as GLAST or EGRET. Let us consider each source of background in turn.

A. Hadronic and electronic

Bergstrom *et al.* [2] use data taken with the Whipple ACT to derive the following expression for the hadronic background:

$$\frac{d\Phi_{\mathrm{had}}}{d\Omega}(E>E_0) = 6.1\times10^{-3}\epsilon_{\mathrm{had}}\left(\frac{E_0}{1\ \ \mathrm{GeV}}\right)^{-1.7} \mathrm{cm}^{-2}\,\mathrm{s}^{-1}\,\mathrm{sr}^{-1}, \tag{11}$$

where ϵ_{had} is intended to take into account improved hadronic rejection expected in future ACTs, but is at present set to unity.

Showers initiated by cosmic-ray electrons are indistinguishable from γ rays. This contribution to the background for ACTs is, according to Ref. [2] (who cite Ref. [36] for this purpose):

$$\frac{d\Phi_{e^-}}{d\Omega} = 3\times10^{-2}\left(\frac{E_0}{1\ \ \mathrm{GeV}}\right)^{-2.3} \mathrm{cm}^{-2}\,\mathrm{s}^{-1}\,\mathrm{sr}^{-1}. \tag{12}$$

B. Diffuse emission

The diffuse γ-ray background is usually taken to be dominated by the galactic [37] or extragalactic [38] contribution, depending on whether the target location is the Galactic Center or at higher latitudes ($b \geqslant 10°$). For example, a fit to the EGRET data [37] at 1 GeV (dominated by the galactic contribution) is given in Ref. [2] as

$$\frac{d\Phi_{\mathrm{diff}}}{d\Omega\, dE} = N_0(l,b)10^{-6}\left(\frac{E_0}{1\ \ \mathrm{GeV}}\right)^{-2.7} \mathrm{cm}^{-2}\,\mathrm{s}^{-1}\,\mathrm{sr}^{-1}\,\mathrm{GeV}^{-1}, \tag{13}$$

where $N_0(l,b)$ is a factor in the range 1–100, with higher values for the central regions of the Galaxy. In Ref. [7], only the extragalactic contribution from EGRET, estimated in Ref. [38], is considered:

$$\frac{d\Phi_{\rm diff}}{d\Omega dE} = (7.32 \pm 0.34) \times 10^{-9} \left(\frac{E_0}{451\ \ {\rm MeV}} \right)^{-2.10 \pm 0.03} {\rm cm}^{-2}\,{\rm s}^{-1}\,{\rm sr}^{-1}\,{\rm MeV}^{-1}$$

$$\approx 1.4 \times 10^{-6} \left(\frac{E_0}{1\ \ {\rm GeV}} \right)^{-2.10 \pm 0.03} {\rm cm}^{-2}\,{\rm s}^{-1}\,{\rm sr}^{-1}\,{\rm GeV}^{-1}. \quad (14)$$

So, the spectral indices of the Galactic and extragalactic contributions are about -2.7 and -2.1, respectively.

However, the separation between the Galactic and extragalactic background is not clear. For example in Ref. [39], the case is made for a very low extragalactic background. Studying the region around the galactic poles ($b \approx 90°$), it seems that, even there, most of the contribution is of galactic origin. In particular, the main contribution is not isotropic but correlated with known galactic tracers. The EGRET Collaboration concede that *any* simple model for the diffuse background is unlikely to work for all points in the sky and at all energies [40].

To be conservative, we normalize the flux to the EGRET data above 1 GeV and choose a spectral index of -2.1 which is the worst case:

$$\frac{d\Phi_{\rm diff}}{d\Omega dE} = \mathcal{N} \left(\frac{E}{1\ \ {\rm GeV}} \right)^{-2.1}. \quad (15)$$

The emission above 1 GeV in the region of our interest can be downloaded from the EGRET website [41]. The exact values for the diffuse emission are 6.7×10^{-7} cm^{-2} s^{-1} sr^{-1} at the location of the Draco dSph ($l = 86.4°$, $b = 34.7°$), 3.18×10^{-6} cm^{-2} s^{-1} sr^{-1} at the location of the Sagittarius dSph ($l = 5.6°$, $b = -14.1°$), 3.87×10^{-6} cm^{-2} s^{-1} sr^{-1} at the location of the Canis Major dSph ($l = 240°$, $b = -8°$), and 1.2×10^{-4} cm^{-2} s^{-1} sr^{-1} at the Galactic Center.

The diffuse emission is the only background for satellite experiments. Its large variation with galactic coordinates can make a weak source in Draco relatively brighter than strong emission from the Galactic Center, overwhelming the numbers in Table III. For ACTs, however, the hadronic and electronic backgrounds are much larger and independent of galactic coordinates, so the hierarchy from Table III is retained. So, this raises the possibility that the Sagittarius dSph might have a higher signal-to-noise ratio with ACTs, but the Draco dSph is more clearly seen from satellites.

V. THE DETECTORS

A. Minimum detectable flux

For the dSphs, the minimum detectable flux Φ_γ is determined using the prescription that, for an exposure of t seconds made with an instrument of effective area $A_{\rm eff}$ and angular acceptance $\Delta\Omega$, the significance of the detection must exceed 5σ:

$$\frac{\Phi_\gamma \sqrt{\Delta\Omega A_{\rm eff} t}}{\sqrt{\Phi_\gamma + \Phi_{\rm bg}}} \geqslant 5. \quad (16)$$

Here, Φ_γ denotes the neutralino annihilation flux in cm^{-2} s^{-1} sr^{-1}, while $\Phi_{\rm bg}$ is the background flux. Any detector sees some photons from both dark matter annihilation and background, so the error in the measurement is $\propto \sqrt{\Phi_\gamma + \Phi_{\rm bg}}$ and not $\propto \sqrt{\Phi_\gamma}$. As pointed out in Ref. [42], the use of the latter formula overestimates the significance of any detection.

When studying the signal from discrete γ lines, $d\Phi_{\rm bg}/d\Omega$ is the background flux falling under the annihilation line. If the background has a differential spectrum $d^2\Phi_{\rm bg}/d\Omega dE = N_0 E^{-\delta}$, and if the energy resolution of the instrument is σ_E/E, then the background under a line at energy E_0 (i.e., in the interval $[E_0 - \sigma_E, E_0 + \sigma_E]$ containing 68% of the signal) is given by [2]

$$\frac{d\Phi_{\rm bg}}{{\rm d}\Omega} = \frac{N_0}{\delta - 1} E_0^{-\delta+1} \times \eta(\sigma_E/E, \delta), \quad (17)$$

with

$$\eta(\sigma_E/E, \delta) = \frac{1}{(1 - \sigma_E/E)^{1-\delta}} - \frac{1}{(1 + \sigma_E/E)^{1-\delta}}. \quad (18)$$

For ACTs, the background is the sum of three different power laws; for satellites, only the diffuse background is needed.

In the literature, a number of different algorithms are used to define a detection of dark matter annihilation. Some authors additionally require a minimum number of detected photons, though this number is set somewhat arbitrarily. In Ref. [2], the minimum number is 25 for ACTs and 10 for satellite experiments; in Ref. [43], it is 100 for ACTs. In Ref. [7], no minimum number of detected photons is required, which allows the possibility of a high significance detection with a tiny number of received photons. In Ref. [8], a completely different strategy altogether is used: constraints on supersymmetric parameter space are found by requiring that Draco's flux be less than the least significant detection (the Large Magellanic Cloud at 4σ [44]) above 1 GeV, resulting in a minimum flux for detection of 10^{-8} cm^{-2} s^{-1}. In this way, the noise enters *linearly* into the expression. This explains why Tyler [8] excludes a large region in mSUGRA parameter space from the non-detection of dSphs, despite the fact that the values of the integral (7) towards the dSphs are quite low.

TABLE V. Performance of the γ-ray detectors. Numbers quoted correspond to 5σ sensitivity after 100 h of observation for ACTs and 1 yr for GLAST.

	High energy γ-ray detectors				
	HESS (I)	VERITAS	MAGIC	EGRET	GLAST
Energy	40 GeV-10 TeV	50 GeV-10 TeV	30 GeV-10 TeV	20 MeV-30 GeV	20 MeV-300 GeV
σ_E/E	$\approx 10\%$	$\approx 15\%$	$\approx 20\%$	$<10\%$	$\approx 5\% > 10$ GeV
$A_{\rm eff}$ (cm^2)	4×10^8 (>100 GeV)	4×10^8 (>100 GeV)	4×10^8 (>100 GeV)	1.5×10^3	10^4
$\Phi_{\rm min}$ (cm^{-2} s^{-1})	8×10^{-12} (>100 GeV)	9×10^{-12} (>100 GeV)	$\approx 10^{-11}$ (>100 GeV)	10^{-7} (>100 MeV)	3×10^{-9} (>100 MeV)
Ang. res. (single γ)	$<0.1°$ at 100 GeV	$<0.1°$ at 100 GeV	$\approx 0.2°$	$<5.8°$ at 100 MeV	2° at 100 MeV 0.1° at 10 GeV
Field of view	$4.3°-5°$	3.5°	$\approx 5°$	0.5 sr	2.4 sr

B. Performance of the detectors

The detector characteristics of the different experiments are summarized in Table V. For definiteness, we use $\Delta\Omega = 10^{-5}$ sr$\approx 0.1°$ for the angular average when considering ACT's (appropriate for energies ~ 100 GeV) or GLAST (10 GeV), and $\Delta\Omega = 10^{-3}$ sr$\approx 1°$ for EGRET (10 GeV). Also important is the observation time, which is chosen as $t \approx 1$ yr for satellites. For the next generation ACTs, assuming four telescopes, we use an observation time $t \approx 100$ h and an exposure $A_{\rm eff} = 4\times10^8$ cm^2. This seems reasonable, as CANGAROO [45] and the last phase of HESS [46] will have four telescopes, while VERITAS will have as many as seven [3]. MAGIC [47] uses a single 17 m mirror and has roughly the same performance as next-generation ACTs, but with a reduced threshold of 30 GeV.

VI. RESULTS

The following plots show the parts of the supersymmetric parameter space that can be probed through the detection of a γ-ray signal from neutralino annihilations. We typically show the region to which GLAST and a generic second generation ACT will be sensitive. The plots found in Ref. [2] show the γ-ray flux in cm^{-2} s^{-1} against photon energy. They are not appropriate for depicting the exclusion limits from observations of different parts of the sky because the flux changes and hence so do the points representing theoretical models. We prefer to use the type of plot presented in Ref. [7] with $N_\gamma\langle\sigma v\rangle$ (which depends exclusively on the particle physics model) versus m_χ (although other quantities could be used as well).

From Eq. (16), we write the condition for detection in a more convenient way for the plots:

$$N_\gamma\langle\sigma v\rangle \geqslant \frac{4\pi m_\chi^2}{\langle J\rangle}\,\frac{25+\sqrt{625+100\Delta\Omega A_{\rm eff} t\Phi_{\rm bg}}}{2\Delta\Omega A_{\rm eff} t}. \quad (19)$$

Here, we see that increasing the angular acceptance $\Delta\Omega$ can increase the signal to noise ratio. In fact, if both signal and background are constant, the significance increases (and the minimum value of $N_\gamma\langle\sigma v\rangle$ that can be probed decreases) as $\sqrt{\Delta\Omega}$. However, the signal is not constant as Table III shows, and the angular acceptance that maximizes the significance does not necessarily coincide with the minimum angular resolution of the detector. So the optimal strategy is to scan between the minimum angular resolution and the maximum field of view, choosing the field for which the signal to noise ratio is maximized. This depends on the position in the sky and on the type of profile. For instance, the distant Draco looks similar to a point source and the maximum signal is for the smallest angle possible. For Sagittarius, the optimal angle is 0.4° for cored profiles and the smallest possible for cusped profiles. In order not to put too many lines in the plot, we have avoided drawing all the halo types and show only the extreme cases.

A. Discrete lines

The annihilation of two neutralinos gives rise to two photons with energy $E_\gamma \approx m_\chi$. The region probed by the different experiments is shown in Fig. 1. Also shown are ~ 1500

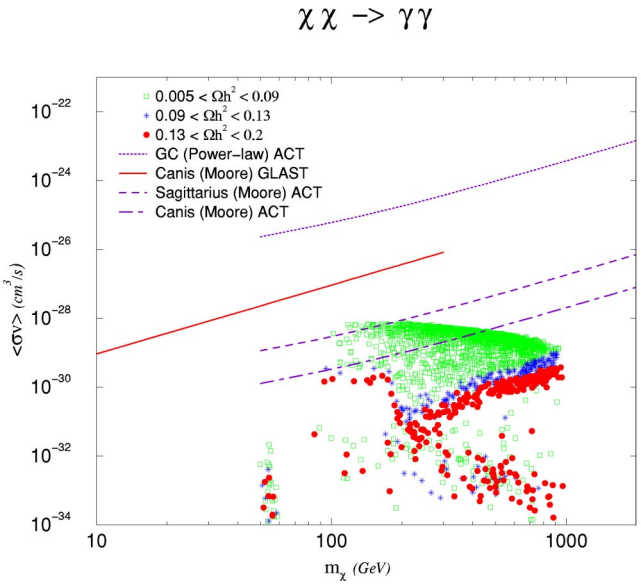

FIG. 1. Exclusion limits for the discrete line $\chi\chi\to\gamma\gamma$. For all the experiments, only the most favorable cases are shown. The square (green), round (red), and star (blue) points correspond to mSUGRA models with $\Omega_{\rm CDM}h^2$ in the range 0.005–0.2, as discussed in Sec. III A. The round (red) points satisfy the more stringent WMAP constraints $0.09 < \Omega_{\rm CDM}h^2 < 0.13$. The exclusion limits for $\chi\chi\to Z\gamma$ are very similar and not shown here.

points in the mSUGRA parameter space that comply with all the accelerator limits (including $b \to s\gamma$, $(g-2)_\mu$ and other accelerator limits [48] that are incorporated in DARKSUSY). All the points, bar five, have spin-independent cross section with protons or neutrons below 10^{-6} pb, thus compatible with limits set by the Edelweiss nuclear recoil detector, but not the disputed signal claimed by the DAMA experiment [49]. Also, the upward-going, neutrino-originated, muon showers have a flux of $\leqslant 10^4$ km^{-2} yr^{-1} (which according to Kurylov and Kamionkowski [50] is the limit set by super-Kamiokande).

As the figure shows, the discrete annihilation line is very unlikely to be observed, even with the next generation instruments. It is just about detectable for the most promising targets under the most optimistic assumptions—the Sagittarius or the Canis Major dSph galaxies assuming a Moore profile and using next generation ACTs. Other possible models (such as NFW or cored profiles) and targets (such as the Galactic Center) are much less propitious still. For GLAST, only one line is shown—namely, that for the Canis Major dSph, but even this lies above all physical mSUGRA models and so provides no constraints. In particular, monochromatic lines from the Galactic Center are not visible to GLAST. The difference between this work and that of Ref. [2] is that the latter authors took a very high dark matter concentration in the center (the profile is just NFW, but the constant in front is set to ensure maximal flux given two weak constraints on the mass and the rotation curve). This causes the γ-ray flux in monochromatic lines from the Galactic Center as computed by Ref. [2] to be over two orders of magnitude greater than the values obtained in this paper.

B. Continuum emission

The continuum emission comes from hadronization and subsequent pion decay. The program DARKSUSY [33] uses results from the PYTHIA code [51] to compute the photon multiplicity for each neutralino annihilation. Experimental sensitivities are shown in Fig. 2 for continuum emission above 1 and 50 GeV.

The continuum emission above 1 GeV can yield some constraints. Although we have computed the curves for four targets (Draco, Sagittarius, Canis Major, and the Galactic Center) and for the full range of models in Sec. II, we give only the most promising results in the figures. The Draco, Sagittarius, and Canis Major dSphs may yield interesting constraints—but only if their dark halo profiles are strongly cusped (the Moore and the NFW profiles both rule out some supersymmetric models). Unlike the case of the Milky Way, cusped profiles are still possible for the dSphs. Notice, however, that substituting cored power-law models for NFW or Moore profiles causes the exclusion limit to move well above the supersymmetric parameter space of interest. For $E_\gamma > 1$ GeV, only curves for GLAST are drawn, as ACTs are insensitive at such low energies.

Also shown in the upper panel of Fig. 2 is a line corresponding to the Milky Way observed at medium latitudes with the wide field of view of GLAST, as first suggested by Stoehr *et al.* [6]. (This line lies almost exactly on top of the line for the Sagittarius dSph in the upper panel.) Here the Galaxy has been modelled with an isothermal power-law model, as opposed to the cusped models preferred by Stoehr *et al.* We agree therefore with the suggestion of Stoehr *et al.* that this is a promising target, as irrespective of whether the Galaxy is cusped or cored, there are always useful constraints on the supersymmetric parameters. Unfortunately, this attractive option is only available to GLAST and not for ACTs.

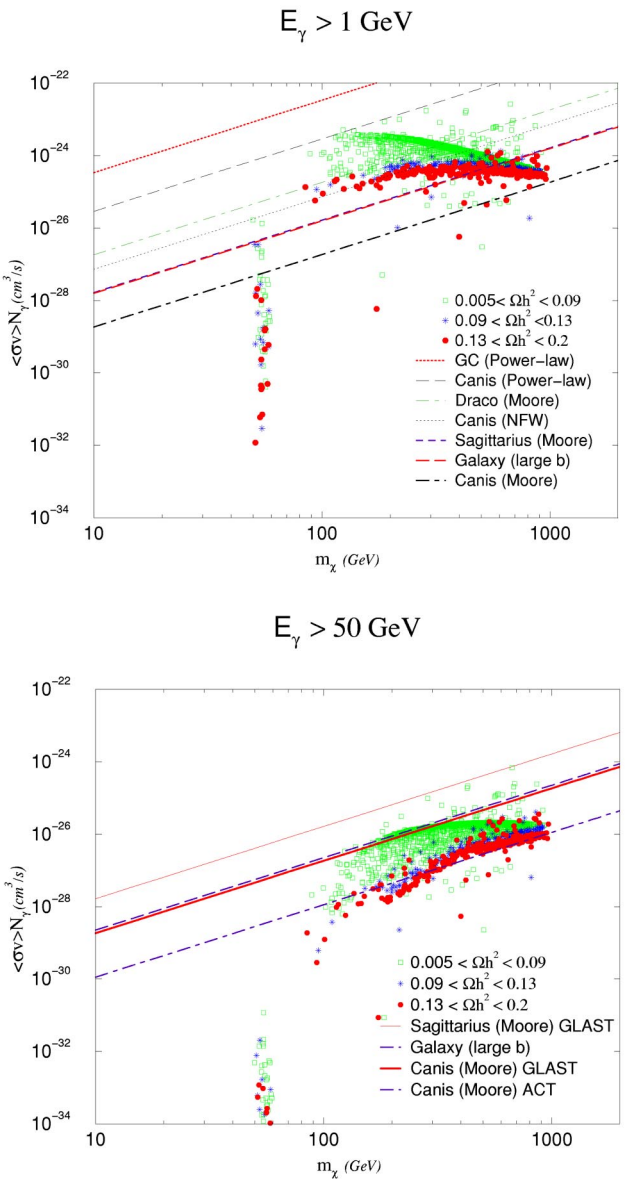

FIG. 2. Exclusion limits for continuum γ-ray emission above 1 GeV (top) and 50 GeV (bottom). Only the most favorable cases are shown. For $E_\gamma > 1$ GeV, only curves for GLAST are drawn, as ACTs are insensitive at such low energies. Above 50 GeV, curves are shown for both GLAST and second generation ACTs. The square (green), round (red), and star (blue) points correspond to mSUGRA models with $\Omega_{\rm CDM}h^2$ in the range 0.005–0.2, as discussed in Sec. III A. The round (red) points satisfy the more stringent WMAP constraints $0.09 < \Omega_{\rm CDM}h^2 < 0.13$.

The lower panel of Fig. 2 shows the prospects for detection of continuum emission above 50 GeV. For ACTs, the Canis dSph is the best target, though a detectable signal will again only be measured if the density profile is strongly cusped. For GLAST, the Galaxy at medium latitudes again leads to some constraints, though not as strong as when continuum emission above 50 GeV is studied.

VII. CONCLUSIONS

If the dark matter present in the Universe is composed at least in part by the lightest supersymmetric particle, then this could manifest itself via γ-ray emission from pair annihilations. It is clearly important to estimate the likely magnitude of the neutralino annihilation signal. It is also important to identify the likely locations and spectral régimes in which the signal should be sought. This paper has provided new estimates of the signal towards the Galactic Center and the nearby dwarf spheroidals using a variety of models.

There have been a number of recent calculations predicting that the neutralino annihilation flux from the inner Galaxy will be detectable with forthcoming satellites such as GLAST and with second generation atmospheric Cerenkov telescopes (ACTs) [2,6]. These calculations assume that the cusped Navarro-Frenk-White (NFW) models for the Milky Way halo hold good. This assumption is in contradiction with a substantial body of astrophysical evidence about the inner galaxy [13–15]. In any case, even if the Milky Way halo was originally of NFW form, the formation of the disk and bulge will have reprocessed the primordial dark matter distribution [16]. In contradiction with earlier results, we do not find the prospects of detecting the annihilation flux from the Galactic Center to be particularly promising. In particular, the γ-ray line coming from the $\gamma\gamma$ and $Z\gamma$ final states is not detectable either with second generation ACTs or with the GLAST satellite. We caution that many of the recent estimates of high flux are sensitively dependent on the assumptions made regarding the innermost structure of the dark halo. Even the best numerical simulations have difficulty in resolving structures on scales less than 1 kpc, and so the inner profile is always found by extrapolation.

The high mass-to-light ratios of the local group dwarf spheroidals (dSphs) makes them attractive targets. Cusped profiles such as NFW are not presently ruled out for dSphs such as Sagittarius or Draco. It may be that the visible dwarf galaxy lies entirely within the central parts of a cusped dark matter halo. If so, then the optimum targets are the Sagittarius and Canis Major dSphs. The detection of monochromatic lines is still extremely difficult, but the GLAST satellite may detect excess continuum γ ray emission. This is of course a less distinctive feature than a sharp line. In particular, if the Sagittarius or Canis Major dSphs have a strongly cusped dark halo profile ($\rho \sim r^{-1.5}$ or $\rho \sim r^{-1}$), then some regions of supersymmetric parameter space can be ruled out. Again, however, this conclusion only holds good if the dark halo profile is cusped. Using a cored isothermal-like model for the dark halo, even the Sagittarius and Canis Major dSphs may be invisible to GLAST and second generation ACTs.

Unlike Bergstrom *et al.* [2], we do not find the Galactic Center to be a promising location. Partly, this is because we believe that the Milky Way does *not* have a strongly cusped profile based on the available astrophysical evidence [13–15]. Partly, this is because Bergstrom *et al.* chose a generous overall normalization anyhow—they used the NFW model corresponding to the maximum flux which satisfies two weak constraints on the mass and the rotation curve. Accordingly, the local dark matter density is as high as ~ 0.6 GeV cm^{-3} in their model. When the circular velocity curve of such a halo is combined with that for the disk and bar, then it necessarily violates the constraint on the Galactic rotation curve in the inner parts. One important caveat of our results, however, is that the possible effects of a central black hole are not included in our calculations. Here, we merely note that the observability of any expected signal depends on the manner in which the black hole grows [53,54].

Stoehr *et al.* [6] have also recently emphasised that the γ-ray emission from the Galactic Center may have been overestimated by the use of too strongly cusped profiles. They suggest that the galaxy at moderate latitudes ($|b| > 10°$) may also be a good target for detecting the continuum emission (they do not study the line emission). This is not really an option for ACTs with their small field of view. However, it is an attractive possibility for GLAST, as the continuum emission is detectable irrespective of uncertainties in halo structure. For ACTs, the best targets remain the Sagittarius and Canis Major dSphs.

Very recently, the Large Magellanic Cloud (LMC) has been suggested as another likely target [29]. Judging from Ref. [52], the average mass to light ratio of the LMC within 8.9 kpc is only ~ 3 (as opposed to ~ 100 for the compact dSphs). This is an upper limit to the central mass to light ratio. In other words, much as in the Milky Way, dark matter dominates the outer parts of the LMC and is responsible for the asymptotic flatness of the ratio curve. However, the central parts of the LMC are dominated by the luminous bar and disk. The assumption that the dark halo dominates the gravitational potential everywhere is therefore not valid. Hence, the procedure used in Ref. [29] of fitting the rotation curve to a NFW dark halo is flawed. The gravitational potential of the gas and stellar disk and bar simply cannot be ignored in the central regions.

ACKNOWLEDGMENTS

We are grateful to I. de la Calle, M. Martinez, M. Ramage and C. Tyler for useful communications. We thank Simon White for critical comments on the draft version.

[1] G. Jungman, M. Kamionkowski, and K. Griest, Phys. Rep. **267**, 195 (1996).
[2] L. Bergström, P. Ullio, and J.H. Buckley, Astropart. Phys. **9**, 137 (1998).
[3] http://veritas.sao.arizona.edu/
[4] http://www-glast.stanford.edu/
[5] J.E. Taylor and J. Silk, Mon. Not. R. Astron. Soc. **339**, 505 (2003).
[6] F. Stoehr, S.D. White, V. Springel, G. Tormen, and N. Yoshida, Mon. Not. R. Astron. Soc. **345**, 1313 (2003).
[7] E.A. Baltz, C. Briot, P. Salati, R. Taillet, and J. Silk, Phys. Rev. D **61**, 023514 (2000).
[8] C. Tyler, Phys. Rev. D **66**, 023509 (2002).
[9] B. Moore, F. Governato, T. Quinn, J. Stadel, and G. Lake, Astrophys. J. **499**, L5 (1998).
[10] J.F. Navarro, C.S. Frenk, and S.D. White, Astrophys. J. **490**, 493 (1997).
[11] L. Bergström, J. Edjsö, P. Gondolo, and P. Ullio, Phys. Rev. D **59**, 043506 (1999).
[12] C. Cálcáneo-Roldan and B. Moore, Phys. Rev. D **62**, 123005 (2000);
[13] N. W. Evans, in *IDM 2000*: *The Third International Conference on the Identification of Dark Matter*, edited by N. Spooner and V. Kudraytsev (World Scientific, Singapore, 2001), p. 85.
[14] J.J. Binney and N.W. Evans, Mon. Not. R. Astron. Soc. **327**, L27 (2001).
[15] V. Debattista and J.A. Sellwood, Astrophys. J. **493**, L5 (1998).
[16] J.J. Binney, O.E. Gerhard, and J. Silk, Mon. Not. R. Astron. Soc. **321**, 471 (2001).
[17] W.J.G. de Blok, S.S. McGaugh, A. Bosma, and V.C. Rubin, Astrophys. J. **552**, L23 (2001).
[18] F.C. van den Bosch and R.A. Swaters, Mon. Not. R. Astron. Soc. **325**, 1017 (2001).
[19] S. Blais-Ouellette, C. Carignan, P. Amram, and S. Côté, Astrophys. J. **118**, 2123 (1999).
[20] J.T. Kleyna, M.I. Wilkinson, G. Gilmore, and N.W. Evans, Astrophys. J. **588**, L21 (2003); **589**, L59(E) (2003).
[21] J.T. Kleyna, M.I. Wilkinson, N.W. Evans, and G. Gilmore, Astrophys. J. **563**, L115 (2001).
[22] R.A. Ibata, R.F.G. Wyse, G. Gilmore, M.J. Irwin, and N.B. Suntzeff, Astrophys. J. **113**, 634 (1997).
[23] N.F. Martin, R.A. Ibata, M. Bellazzini, M.J. Irwin, G.F. Lewis, and W. Dehnen, Mon. Not. R. Astron. Soc. **348**, 12 (2004).
[24] N.W. Evans, Mon. Not. R. Astron. Soc. **260**, 191 (1993); **267**, 333 (1994).
[25] J. Binney, S. Tremaine, *Galactic Dynamics* (Princeton University Press, Princeton, 1987), Sec. 4.2.
[26] M.I. Wilkinson, J. Kleyna, N.W. Evans, and G. Gilmore, Mon. Not. R. Astron. Soc. **330**, 778 (2002).
[27] J.T. Kleyna, M.I. Wilkinson, N.W. Evans, and G. Gilmore, Mon. Not. R. Astron. Soc. **330**, 792 (2002).
[28] P. Blasi and R. Sheth, Phys. Lett. B **486**, 233 (2000).
[29] A. Tasitsiomiu, J. Gaskins, and A.V. Olinto, astro-ph/0307375.
[30] M.I. Wilkinson and N.W. Evans, Mon. Not. R. Astron. Soc. **310**, 645 (1999).
[31] H.P. Nilles, Phys. Rep. **110**, 1 (1984).
[32] B.C. Allanach, Comput. Phys. Commun. **143**, 305 (2002); http://allanach.home.cern.ch/allanach/softsusy.html
[33] P. Gondolo, J. Edsjö, L. Bergstrom, P. Ullio, and E. A. Baltz, http://www.physto.se/~edsjo/darksusy/
[34] WMAP Collaboration, D.N. Spergel *et al.*, Astrophys. J., Suppl. **148**, 175 (2003).
[35] A. Blanchard, M. Douspis, M. Rowan-Robinson, and S. Sarkar, Astron. Astrophys. **412**, 35 (2003).
[36] M. S. Longair, *High Energy Astrophysics* (Cambridge University Press, Cambridge, 1992).
[37] EGRET Collaboration, S.D. Hunter *et al.*, Astrophys. J. **481**, 205 (1997).
[38] EGRET Collaboration, P. Sreekumar *et al.*, Astrophys. J. **494**, 523 (1998).
[39] U. Keshet, E. Waxman, and A. Loeb, astro-ph/0306442.
[40] EGRET Collaboration, R.C. Hartman *et al.*, Astrophys. J., Suppl. **123**, 79 (1999).
[41] http://cossc.gsfc.nasa.gov/egret/
[42] T.-P. Li and Y.-Q. Ma, Astrophys. J. **272**, 317 (1983).
[43] F.A. Aharonian, W. Hofmann, A.K. Konopelko, and H.J. Völk, Astropart. Phys. **6**, 369 (1997).
[44] R.C. Lamb and D.J. Macomb, Astrophys. J. **488**, 872 (1997).
[45] http://www.physics.adelaide.edu.au/astrophysics/cangaroo.html
[46] http://www.mpi-hd.mpg.de/hfm/HESS/HESS.html
[47] M. Martinez, Proceedings of the XXVI ICRC 5, 219, 1999; http://hegra1.mppmu.mpg.de/MAGICWeb/
[48] Particle Data Group, K. Hagiwara *et al.*, Phys. Rev. D **66**, 010001 (2002).
[49] http://cdms.berkeley.edu/limitplots/
[50] A. Kurylov and M. Kamionkowski, Phys. Rev. D **69**, 063503 (2004).
[51] T. Sjostrand, L. Lonnblad, S. Mrenna, and P. Skands, hep-ph/0308153.
[52] R.P. van der Marel, D.R. Alves, E. Hardy, and N.B. Suntzeff, Astron. J. **124**, 2639 (2002).
[53] P. Gondolo and J.I. Silk, Phys. Rev. Lett. **83**, 1719 (1999).
[54] D. Merritt, M. Milosavljevic, L. Verde, and R. Jimenez, Phys. Rev. Lett. **88**, 191301 (2002).